

Born effective charge removed anomalous temperature dependence of lattice thermal conductivity in monolayer GeC

San-Dong Guo

School of Physics, China University of Mining and Technology, Xuzhou 221116, Jiangsu, China

Due to potential applications in nano- and opto-electronics, two-dimensional (2D) materials have attracted tremendous interest. Their thermal transport properties are closely related to the performance of 2D materials-based devices. Here, the phonon transports of monolayer GeC with a perfect planar hexagonal honeycomb structure are investigated by solving the linearized phonon Boltzmann equation within the single-mode relaxation time approximation (RTA). Without inclusion of Born effective charges (Z^*) and dielectric constants (ϵ), the lattice thermal conductivity (κ_L) almost decreases linearly above 350 K, deviating from the usual $\kappa_L \sim 1/T$ law. The underlying mechanism is because the contribution to κ_L from high-frequency optical phonon modes increases with increasing temperature, and the contribution exceeds one from acoustic branches at high temperature. These can be understood by huge phonon band gap caused by large difference in atom mass between Ge and C atoms, which produces important effects on scattering process involving high-frequency optical phonon. When considering Z^* and ϵ , the phonon group velocities and phonon lifetimes of high-frequency optical phonon modes are obviously reduced with respect to ones without Z^* and ϵ . The reduced group velocities and phonon lifetimes give rise to small contribution to κ_L from high-frequency optical phonon modes, which produces the traditional $\kappa_L \sim 1/T$ relation in monolayer GeC. Calculated results show that the isotope scattering can also reduce anomalous temperature dependence of κ_L in monolayer GeC. Our works highlight the importance of Z^* and ϵ to investigate phonon transports of monolayer GeC, and motivate further theoretical or experimental efforts to investigate thermal transports of other 2D materials.

PACS numbers: 72.15.Jf, 71.20.-b, 71.70.Ej, 79.10.-n

Keywords: Lattice thermal conductivity; Monolayer; Born effective charge

Email:sandongyuwang@163.com

I. INTRODUCTION

Since the successful synthesis of graphene¹, 2D materials have attracted increasing attention due to potential applications in electronics, spintronics and optoelectronics²⁻⁹. Thermal management is a significant factor for these applications¹⁰. To efficiently dissipate heat in electronic devices, a high thermal conductivity is required, while a low lattice thermal conductivity is beneficial to thermoelectric applications, to achieve good thermoelectric performance^{11,12}. Diverse anisotropy of phonon transport in group IV-VI monolayer is predicted by solving the Boltzmann transport equation¹³. Phonon transport properties of group-IV and -VA element monolayers have been performed theoretically¹⁴⁻¹⁶. The κ_L of transition metal dichalcogenide (TMD) and Janus TMD monolayers have been systematically studied by phonon Boltzmann transport equation approach^{17,18}. Strain effects on thermal transports of Sb monolayer¹⁹, group-IV monolayers²⁰ and 2D penta-structures materials²¹ have also been studied, showing diverse strain dependence, such as monotonously increasing or decreasing and up-and-down behaviors with increasing tensile strain.

For most bulk and 2D materials, the temperature-dependent κ_L follows the relation of $\kappa_L \sim 1/T$. Recently, anomalously temperature-dependent κ_L of monolayer ZnO and GaN is predicted by a first-principles study^{22,23}, which is due to the huge phonon band gap in their phonon dispersions. The predicted room-temperature κ_L of monolayer ZnO and GaN is $4.5 \text{ Wm}^{-1}\text{K}^{-1}$ with

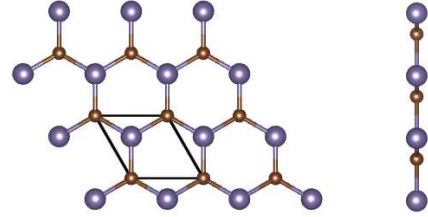


FIG. 1. (Color online) The top (Left) and side (Right) view of monolayer GeC, and the frame surrounded by a black box is unit cell. The large and small balls represent Ge and C atoms, respectively.

the thickness of 3.04 \AA and $14.93 \text{ Wm}^{-1}\text{K}^{-1}$ with the thickness of 3.74 \AA , respectively. The SiC monolayer has the same perfect planar hexagonal honeycomb structure with ZnO and GaN, but the κ_L of SiC monolayer follows the conventional $1/T$ law²⁴, which may be due to small phonon band gap. For GeC monolayer with the same structure, a large phonon band gap can be observed due to a large difference in atom mass between Ge and C atoms²⁵. The similar anomalous temperature dependence of κ_L may also exist in monolayer GeC. In this work, based on first-principles calculations, the phonon transport properties of monolayer GeC are investigated by solving the linearized phonon Boltzmann equation. When neglecting Z^* and ϵ , the κ_L deviates from the usual $\kappa_L \sim 1/T$ law. The κ_L above 200 K is much higher than the expected κ_L predicted from the general $\kappa_L \sim 1/T$ law. The large deviation stems from the high-frequency opti-

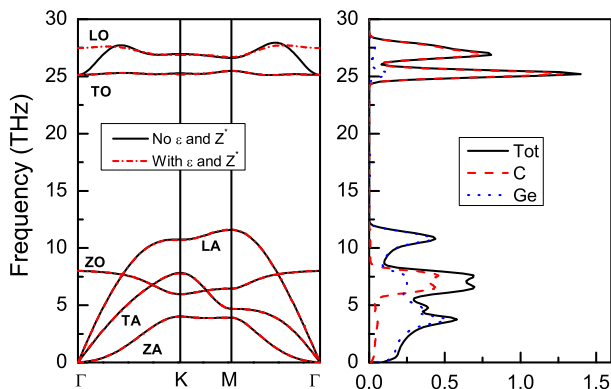


FIG. 2. (Color online) Phonon band structures of monolayer GeC with or without ε and Z^* , along with the total and partial DOS without ε and Z^* .

cal phonon modes, whose contribution to κ_L increases with increasing temperature, and eventually dominates κ_L . With inclusion of Z^* and ε , the phonon group velocities and phonon lifetimes of high-frequency optical phonon modes are obviously reduced, which gives rise to small contribution to κ_L from high-frequency optical phonon modes, producing the traditional $\kappa_L \sim 1/T$ relation in monolayer GeC. It is found that the isotope scattering can also reduce anomalous temperature dependence of κ_L in monolayer GeC.

The rest of the paper is organized as follows. In the next section, we shall give our computational details about phonon transport. In the third section, we shall present phonon transport of monolayer GeC. Finally, we shall give our discussion and conclusions in the fourth section.

II. COMPUTATIONAL DETAIL

All first-principles calculations are carried out based on the density functional theory (DFT) using the projected augmented wave (PAW) method, and the generalized gradient approximation of the Perdew-Burke-Ernzerhof (GGA-PBE) is adopted as exchange-correlation energy functional, as implemented in the Vienna ab initio simulation package (VASP)^{26–29}. A plane-wave basis set is employed with kinetic energy cutoff of 700 eV, and the $2s2p$ ($4s4p$) orbitals of C (Ge) atoms are treated as valance ones. To avoid spurious interaction, the unit cell of monolayer GeC is built with the vacuum region of 18 Å along the out-of-plane direction. The energy convergence threshold is set as 10^{-8} eV.

The κ_L of monolayer GeC is calculated by solving linearized phonon Boltzmann equation with the single mode RTA, as implemented in the Phono3py code³⁰. The κ_L can be expressed as:

$$\kappa = \frac{1}{NV_0} \sum_{\lambda} \kappa_{\lambda} = \frac{1}{NV_0} \sum_{\lambda} C_{\lambda} \nu_{\lambda} \otimes \nu_{\lambda} \tau_{\lambda} \quad (1)$$

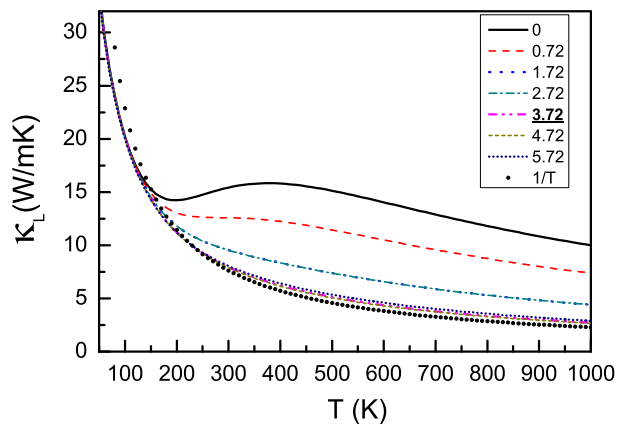


FIG. 3. (Color online) The κ_L of monolayer GeC with or without ε and Z^* as a function of temperature (3.72 and 0); The $\kappa_L \sim 1/T$ relation is plotted for comparison; The κ_L with $|Z^*|$ along xx and yy directions artificially changing from 0.72 to 5.72.

where λ , N and V_0 are phonon mode, the total number of q points sampling Brillouin zone (BZ) and the volume of a unit cell, and C_{λ} , ν_{λ} , τ_{λ} is the specific heat, phonon velocity, phonon lifetime. The phonon lifetime τ_{λ} can be attained by phonon linewidth $2\Gamma_{\lambda}(\omega_{\lambda})$ of the phonon mode λ :

$$\tau_{\lambda} = \frac{1}{2\Gamma_{\lambda}(\omega_{\lambda})} \quad (2)$$

The $\Gamma_{\lambda}(\omega)$ takes the form analogous to the Fermi golden rule:

$$\Gamma_{\lambda}(\omega) = \frac{18\pi}{\hbar^2} \sum_{\lambda' \lambda''} |\Phi_{-\lambda \lambda' \lambda''}|^2 [(f'_{\lambda} + f''_{\lambda} + 1)\delta(\omega - \omega'_{\lambda} - \omega''_{\lambda}) + (f'_{\lambda} - f''_{\lambda})[\delta(\omega + \omega'_{\lambda} - \omega''_{\lambda}) - \delta(\omega - \omega'_{\lambda} + \omega''_{\lambda})]] \quad (3)$$

in which f_{λ} and $\Phi_{-\lambda \lambda' \lambda''}$ are the phonon equilibrium occupancy and the strength of interaction among the three phonons λ , λ' , and λ'' involved in the scattering.

The interatomic force constants (IFCs) are calculated by the finite displacement method. The second-order harmonic (third-order anharmonic) IFCs are calculated using a $5 \times 5 \times 1$ ($4 \times 4 \times 1$) supercell containing 50 (32) atoms with k-point meshes of $4 \times 4 \times 1$. Using the harmonic IFCs, phonon dispersion of monolayer GeC can be attained, using Phonopy package³¹. To compute lattice thermal conductivities, the reciprocal spaces of the primitive cells are sampled using the $100 \times 100 \times 1$ meshes. For 2D material, the calculated lattice thermal conductivity depends on the length of unit cell used in the calculations along z direction³². The lattice thermal conductivity should be normalized by multiplying Lz/d , in which Lz is the length of unit cell along z direction and d is the thickness of 2D material, but the d is not well defined like graphene. In this work, the length of unit cell (18 Å) along z direction is used as the thickness

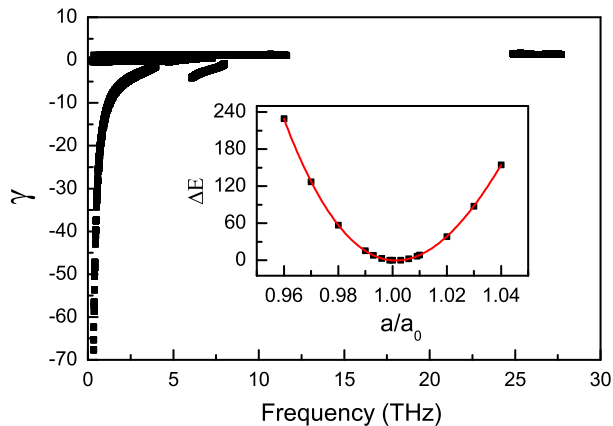


FIG. 4. (Color online) The mode level Grüneisen parameters of monolayer GeC in the first BZ; (Inset) the potential energy well $\Delta E = E_{a/a_0} - E_1$ as a function of a/a_0 .

of monolayer GeC. To make a fair comparison between various 2D monolayers, the thermal sheet conductance can be used, defined as $\kappa_L \times d$.

III. MAIN CALCULATED RESULTS AND ANALYSIS

Monolayer GeC prefers a perfect planar hexagonal honeycomb structure, and similar monolayer structure can be found in graphene, ZnO, GaN and SiC^{22,23,25}. The monolayer GeC can be built by replacing one atom in the unit cell of graphene with Ge atom, and the space symmetry group is $P\bar{6}M2$, being lower than that of graphene ($P6/MMM$). Figure 1 shows the schematic crystal structure of monolayer GeC, and the optimized lattice parameter within GGA-PBE is 3.26 Å. Firstly, the elastic properties of monolayer GeC are studied, and two independent elastic constants C_{11} ($=C_{22}$) and C_{12} due to D_{3h} symmetry can be calculated, and the $C_{66} = (C_{11} - C_{12})/2$. For C_{11} , C_{12} and C_{66} , the calculated value is 159.42 Nm^{-1} , 51.62 Nm^{-1} and 53.90 Nm^{-1} , respectively. These C_{ij} satisfy the Born criteria of mechanical stability. Based on calculated C_{ij} , the 2D Young's moduli Y^{2D} and shear modulus G^{2D} of monolayer GeC³³ are 142.71 Nm^{-1} and 53.90 Nm^{-1} , which are lower than ones of graphene and SiC monolayer^{24,33}. The GeC monolayer is more flexible than graphene and SiC monolayer due to smaller Y^{2D} .

TABLE I. The Z^* of C and Ge atoms and ϵ of monolayer GeC. Except for xx , yy and zz directions, the Z^* and ϵ along other directions are zero.

Direction	$Z^*(\text{C})$	$Z^*(\text{Ge})$	ϵ
xx	-3.72	3.72	2.90
yy	-3.72	3.72	2.90
zz	-0.25	0.25	1.18

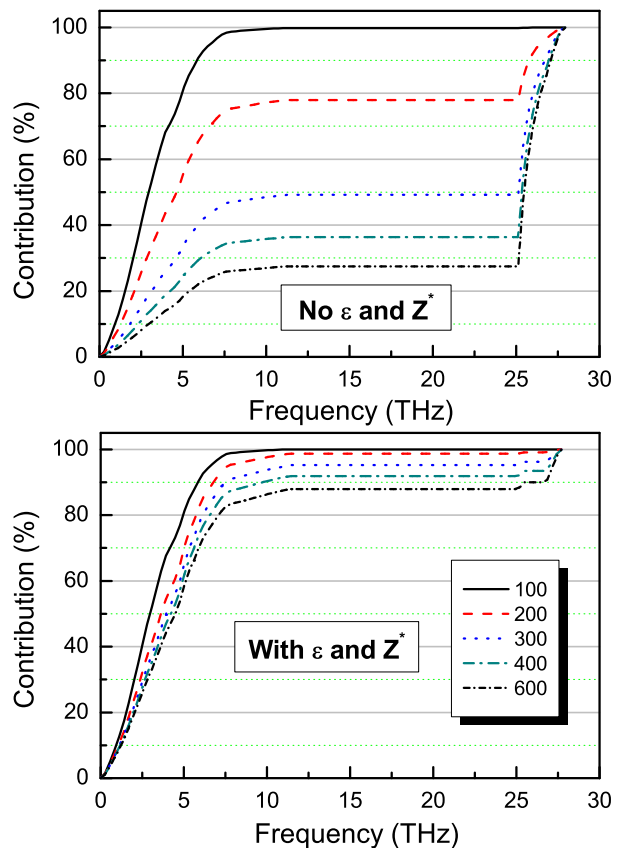


FIG. 5. (Color online) At 100, 200, 300, 400 and 600 K, the ratio between accumulated and total κ_L with respect to frequency with or without ϵ and Z^* .

The calculated phonon dispersion of monolayer GeC along high-symmetry path and total and partial density of states (DOS) are shown in Figure 2. No imaginary frequencies are observed in the phonon dispersion, indicating the thermodynamic stability of monolayer GeC. There are 6 phonon branches due to 2 atoms per unit cell, including 3 acoustic and 3 optical phonon branches. A phonon band gap of 13.52 THz is observed, which separates in-plane transverse optical (TO) and the in-plane longitudinal optical (LO) branches from out-of-plane optical (ZO), in-plane longitudinal acoustic (LA), in-plane transverse acoustic (TA) and out-of-plane acoustic (ZA) branches. It is noted that the phonon band gap is larger than width of acoustic branches (11.61 THz), which has important effects on phonon transport. The large gap can be explained by the Ge atom being much heavier than C atom. It is clearly seen that the ZO branch crosses with the TA and LA branches, which has significant effect on the phonon scattering process. The similar phonon dispersion can also be found in SiC, ZnO and GaN monolayers²²⁻²⁵. However, for monolayer SiC, a phonon band gap of 7.47 THz is very smaller than width of acoustic branches (19.48 THz). Based on the elastic theory, the ZA phonon branch should have quadratic dispersion with the sheet being free of stress^{34,35}. The

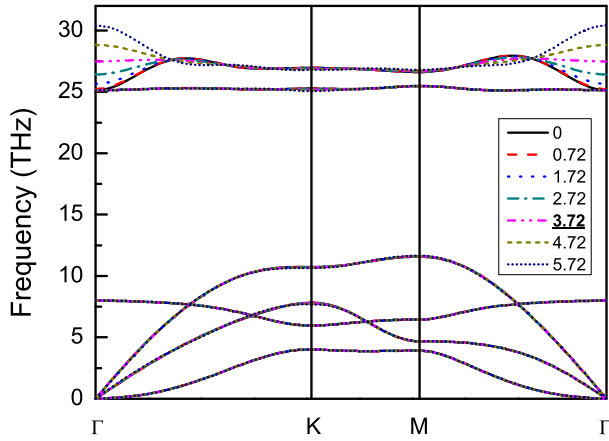


FIG. 6. (Color online) Phonon band structures of monolayer GeC with $|Z^*|$ along xx and yy directions artificially changing from 0 to 5.72.

quadratic ZA branch near the Γ point can be observed for monolayer GeC. However, the TA and LA branches are linear near the Γ point. The partial DOS indicates that optical branches are mainly contributed by the vibrations of C atoms, while acoustic branches are contributed by the vibrations of Ge atoms.

By solving the linearized phonon Boltzmann equation within single-mode RTA method, the intrinsic κ_L of monolayer GeC is calculated, which is plotted in Figure 3 as a function of temperature. The room-temperature κ_L of monolayer GeC is $15.43 \text{ Wm}^{-1}\text{K}^{-1}$ with the thickness of 18 \AA , and the corresponding thermal sheet conductance is 277.74 WK^{-1} , being two orders of magnitude lower than that of graphene (about 12884 WK^{-1})³². To understand the mechanism underlying the low κ_L of monolayer GeC, the mode level Grüneisen parameters of monolayer GeC are shown in Figure 4. It is found that the γ of TO and LO branches is fully positive. For the phonon modes below the gap, both negative and partial positive γ can be observed, and ZA branch shows very large negative γ . However, due to the symmetry-based selection rule, the scattering of ZA branch is largely suppressed. The large γ means strong phonon anharmonicity, which can produce the strong phonon-phonon scattering, leading to the low κ_L of monolayer GeC. To have an explicit view on the phonon anharmonicity from another aspect, the potential energy well of monolayer GeC, defined as potential energy change due to the change of lattice constant ($\Delta E = E_{a/a_0} - E_1$, where E_{a/a_0} and E_1 are the total energies of strained and unstrained systems, respectively), is shown in the inset of Figure 4. It is found that the potential well of monolayer GeC is asymmetric with respect to compressive and tensile strains, which is a direct evidence of the phonon anharmonicity. A three order polynomial curve can be used to fit the potential energy well, and the fitted parameter for the cubic term is -395 eV , and the large cubic term is consistent with the γ .

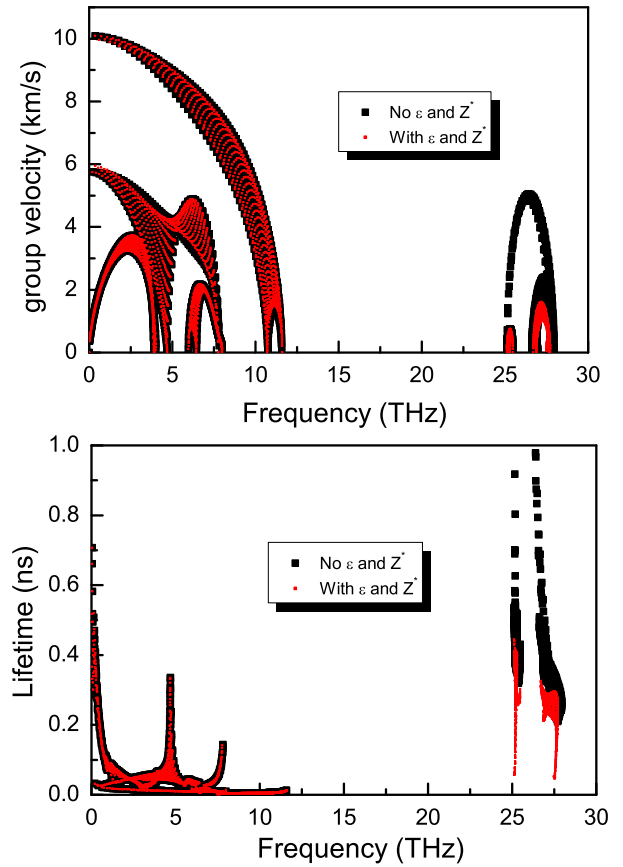


FIG. 7. (Color online) The mode level phonon group velocities and phonon lifetimes (300K) of monolayer GeC in the first BZ with or without ϵ and Z^* .

For the most bulk and 2D materials, the temperature-dependent κ_L follows $\kappa_L \sim 1/T^\alpha$ relationship with α changing from 0.85 to 1.05²². It is very strange that the κ_L of monolayer GeC shows an anomalous linear temperature dependence above about 350 K, which is obviously different from usual picture $\kappa_L \sim 1/T$ relationship. The $\kappa_L \sim 1/T$ relation is also shown in Figure 3 for comparison. To understand the anomalous temperature dependence of κ_L of monolayer GeC, the ratio between accumulated and total κ_L with respect to frequency at 100, 200, 300, 400 and 600 K are plotted in Figure 5. It is clearly seen that, with the temperature increasing, the contribution from LO and TO branches increases. When the temperatures are lower than 300 K, the contribution of phonon modes below the phonon gap is larger than 50%. However, for temperatures higher than 300 K, the LO and TO branches dominate the κ_L with the contribution larger than 50%. If acoustic phonon branches dominate κ_L , the temperature-dependent κ_L would follow $\kappa_L \sim 1/T$ relationship, which can be found for most materials²². So, the anomalous linear temperature dependence of κ_L of monolayer GeC is due to dominant contribution from LO and TO branches, when the temperature is larger than 300 K. Anomalous temperature-

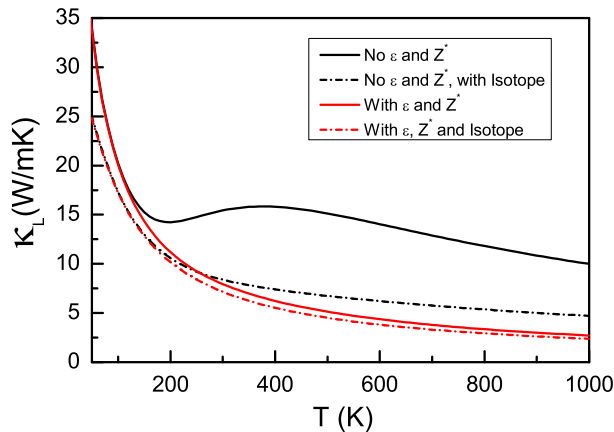


FIG. 8. (Color online) The κ_L of monolayer GeC with or without ε , Z^* and isotope as a function of temperature.

dependent κ_L has been predicted in monolayer ZnO and GaN by Hu et al.²². To achieve the linear temperature dependence of κ_L , Hu et al. propose two conditions: (1) With increased temperature, the contribution to κ_L from optical phonon branches should increase. (2) At high temperature, the optical branches should dominate κ_L . The monolayer GeC indeed satisfies these conditions.

Due to the large charge transfer from Ge to C atom, the long-range electrostatic Coulomb interactions may have important effects on phonon transports of monolayer GeC. The large charge transfer can induce strongly polarized covalent bond, which is also described by Z^* and ε , as given in Table I. The large Z^* and ε can produce large LO-TO splitting (2.35 THz) at the BZ center, as seen in Figure 2. The κ_L with Z^* and ε as a function of temperature is also plotted in Figure 3. It is clearly seen that the relationship between κ_L and T changes from $\kappa_L \sim T$ to $\kappa_L \sim 1/T$. To understand the sudden change, the ratio between accumulated and total κ_L with respect to frequency with Z^* and ε are also plotted in Figure 5 at 100, 200, 300, 400 and 600 K. With increased temperature, the contribution to κ_L from high frequency optical phonon branches increases, but acoustic branches always dominate the κ_L for all temperatures (>80%). With inclusion of Z^* and ε , the condition (2) is broken, so the $\kappa_L \sim T$ relationship disappears.

To have a better understanding about Z^* effects on κ_L , we artificially change $|Z^*|$ along xx and yy directions from 0 to 5.72, and the related phonon dispersions and κ_L are plotted in Figure 6 and Figure 3, respectively. The LO-TO splitting changes from 0 THz to 5.17 THz with increasing $|Z^*|$, and the κ_L gradually deviates from the $\kappa_L \sim T$ relationship. When $|Z^*|$ reaches the true values, $\kappa_L \sim 1/T$ can be observed. To understand the mechanism underlying the sudden change of κ_L , the mode level phonon group velocities and phonon lifetimes (300K) of monolayer GeC with or without ε and Z^* are plotted in Figure 7. The group velocities and phonon lifetimes of phonon modes below the gap have little difference be-

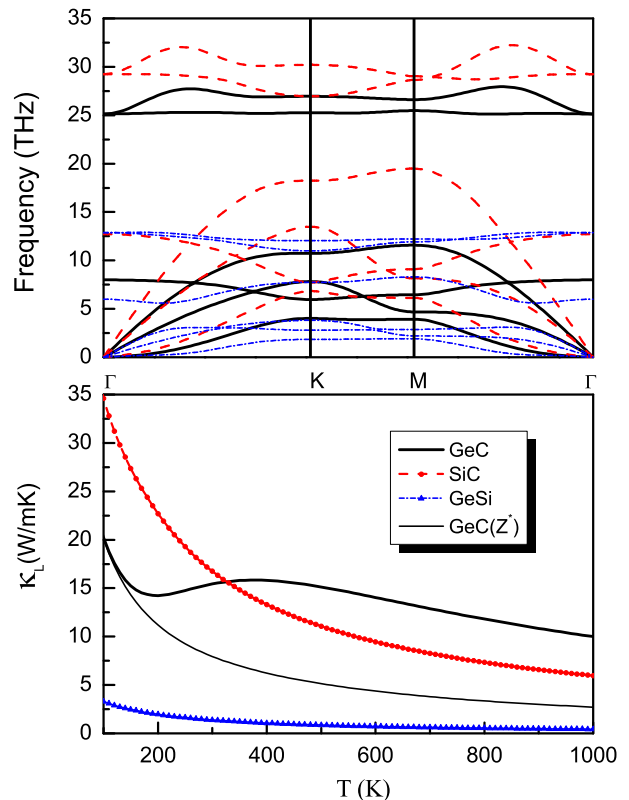


FIG. 9. (Color online) Left: phonon band structures of monolayer GeC, SiC and GeSi without ε and Z^* ; Right: The κ_L of monolayer GeC (without and with ε and Z^*), SiC and GeSi.

tween with and without ε and Z^* . However, for LO and TO branches, the group velocities and phonon lifetimes with ε and Z^* are smaller than ones without ε and Z^* , which dramatically reduces contribution to κ_L from LO and TO branches, and then the normal $\kappa_L \sim 1/T$ relationship is observed in GeC monolayer.

Finally, the phonon-isotope scattering is considered on κ_L , based on the formula proposed by Shin-ichiro Tamura³⁶. The related κ_L with or without ε , Z^* and isotope are plotted in Figure 8. Without inclusion of ε and Z^* , it is clearly seen that the phonon-isotope scattering can also markedly remove $\kappa_L \sim T$ relationship. However, considering ε and Z^* , the phonon-isotope scattering has little effects on κ_L of monolayer GeC. In nanoscale devices, the residual strain usually exists, and the substrate is needed in real applications. Even if the ε and Z^* are neglected, the anomalous temperature dependence of κ_L should depend on the strain and specific substrate.

IV. DISCUSSION AND CONCLUSION

It is interesting to compare phonon transports of monolayer GeC with ones of SiC and GeSi monolayers. The monolayer SiC has also a perfect planar hexagonal honeycomb structure, but monolayer GeSi has a buckled struc-

ture due to the decrease in the overlap between the p_z orbitals²⁵. The phonon band structures and κ_L of monolayer GeC, SiC and GeSi without ε and Z^* are plotted in Figure 9. The ε and Z^* produce little effects on κ_L of monolayer SiC and GeSi, so only the κ_L of monolayer GeC with ε and Z^* is shown in Figure 9. It is clearly seen that anomalous temperature dependence of κ_L is absent in monolayer SiC and GeSi. These can be understood by their phonon dispersions. There is a huge phonon band gap of 13.52 THz (larger than width of acoustic branches [11.61 THz]) in monolayer GeC, which can weaken the scattering between acoustic and high frequency optical phonon modes, producing very large phonon lifetimes of LO and TO branches. For monolayer SiC, a phonon band gap of 7.47 THz is observed (smaller than width of acoustic branches [19.48 THz]), and the LO and TO modes can be effectively scattered with acoustic modes, leading to short phonon lifetimes of LO and TO branches. In monolayer GeSi, there is a very large gap of 7.17 THz (larger than width of acoustic branches [3.81 THz]) between LO/TO and acoustic branches, but ZO branch is in the gap, which provide effective scattering channels for LO and TO branches, giving rise to short phonon lifetimes. When considering ε and Z^* , the order of κ_L is GeSi < GeC < SiC, which is consistent with their atomic mass.

In summary, the phonon transports of monolayer GeC are investigated by the first-principles calculations and semiclassical Boltzmann transport theory. When neglecting ε and Z^* , monolayer GeC possesses anomalously linear temperature dependent κ_L , which is different from the commonly established $\kappa_L \sim 1/T$ relationship. The large deviation is because the contribution to κ_L from LO and TO branches increases with increasing temperature, and eventually dominates the κ_L with T being larger than 300 K. However, considering ε and Z^* , the common $\kappa_L \sim 1/T$ relationship is observed by reduced group velocities and phonon lifetimes of LO and TO branches. It is found that the phonon-isotope scattering can also weaken anomalously linear temperature dependent κ_L in monolayer GeC. This work presents a comprehensive understanding of the phonon transports of monolayer GeC, and sheds light on further studies of phonon transports of other 2D materials.

ACKNOWLEDGMENTS

This work is supported by the National Natural Science Foundation of China (Grant No.11404391). We are grateful to the Advanced Analysis and Computation Center of CUMT for the award of CPU hours to accomplish this work.

-
- ¹ K. S. Novoselov, A. K. Geim, S. V. Morozov, D. Jiang, Y. Zhang, S. V. Dubonos, I. V. Grigorieva and A. A. Firsov, *Science* **306**, 666 (2004).
 - ² M. Chhowalla, H. S. Shin, G. Eda, L. J. Li, K. P. Loh and H. Zhang, *Nature Chemistry* **5**, 263 (2013).
 - ³ R. X. Fei, W. B. Li, J. Li and L. Yang, *Appl. Phys. Lett.* **107**, 173104 (2015).
 - ⁴ S. Ghatak, A. N. Pal and A. Ghosh, *Acs Nano* **5**, 7707 (2011).
 - ⁵ B. Radisavljevic, A. Radenovic, J. Brivio, V. Giacometti and A. Kis, *Nature Nanotechnology* **6**, 147 (2011).
 - ⁶ X. Zong et al. *J. Am. Chem. Soc.* **130**, 7176 (2008).
 - ⁷ J. P. Ji, X. F. Song, J. Z. Liu et al., *Nat. Commun.* **7**, 13352 (2016).
 - ⁸ Z. Y. Al Balushi, K. Wang, R. K. Ghosh, R. A. Vilá, S. M. Eichfeld, J. D. Caldwell, X. Qin, Y.-C. Lin, P. A. DeSario, G. Stone, S. Subramanian, D. F. Paul, R. M. Wallace, S. Datta, J. M. Redwing and J. A. Robinson, *Nat. Mater.* **15**, 1166 (2016).
 - ⁹ M. Topsakal, S. Cahangirov, E. Bekaroglu and S. Ciraci, *Phys. Rev. B* **80**, 235119 (2009).
 - ¹⁰ Z. Yan, G. X. Liu, J. M. Khan and A. A. Balandin, *Nat. Commun.* **3**, 827 (2012).
 - ¹¹ A. M. Marconnet, M. A. Panzer and K. E. Goodson, *Reviews of Modern Physics* **85**, 1295, (2013).
 - ¹² A. I. Hochbaum, R. Chen, R. D. Delgado, W. Liang, E. C. Garnett, M. Najarian, A. Majumdar and P. Yang, *Nature* **451**, 163 (2008).
 - ¹³ G. Qin, Z. Qin, W.-Z. Fang, L.-C. Zhang, S.-Y. Yue, Q.-B. Yan, M. Hu and G. Su, *Nanoscale*, **8**, 11306 (2016).
 - ¹⁴ B. Peng, H. Zhang, H. Z. Shao, Y. F. Xu, G. Ni, R. J. Zhang and H. Y. Zhu, *Phys. Rev. B* **94**, 245420 (2016).
 - ¹⁵ D. C. Zhang, A. X. Zhang, S. D. Guo and Y. F. Duan, *RSC Adv.* **7**, 24537 (2017).
 - ¹⁶ B. Peng, D. Q. Zhang, H. Zhang, H. Z. Shao, G. Ni, Y. Y. Zhu and H. Y. Zhu, *Nanoscale* **9**, 7397 (2017).
 - ¹⁷ X. K. Gu and R. G. Yang, *Appl. Phys. Lett.* **105**, 131903 (2014).
 - ¹⁸ S. D. Guo, *Phys. Chem. Chem. Phys.* **20**, 7236 (2018).
 - ¹⁹ A. X. Zhang, J. T. Liu, S. D. Guo and H. C. Li, *Phys. Chem. Chem. Phys.* **19**, 14520 (2017).
 - ²⁰ Y. D. Kuang, L. Lindsay, S. Q. Shic and G. P. Zheng, *Nanoscale* **8**, 3760 (2016).
 - ²¹ H. K. Liu, G. Z. Qin, Y. Lin and M. Hu, *Nano Lett.* **16**, 3831 (2016).
 - ²² H. M. Wang, G. Z. Qin, G. J. Li, Q. Wang and M. Hu, *Phys. Chem. Chem. Phys.* **19**, 12882 (2017).
 - ²³ Z. Z. Qin, G. Z. Qin, X. Zuo, Z. H. Xiong and M. Hu, *Nanoscale* **9**, 4295 (2017).
 - ²⁴ S. D. Guo and J. T. Liu, arXiv:1706.01025 (2017).
 - ²⁵ H. Sahin, S. Cahangirov, M. Topsakal, E. Bekaroglu, E. Akturk, R. T. Senger, and S. Ciraci, *Phys. Rev. B* **80**, 155453 (2009).
 - ²⁶ G. Kresse, *J. Non-Cryst. Solids* **193**, 222 (1995).
 - ²⁷ G. Kresse and J. Furthmüller, *Comput. Mater. Sci.* **6**, **15** (1996).
 - ²⁸ J. P. Perdew, K. Burke and M. Ernzerhof, *Phys. Rev. Lett.* **77**, 3865 (1996).
 - ²⁹ G. Kresse and D. Joubert, *Phys. Rev. B* **59**, 1758 (1999).
 - ³⁰ A. Togo, L. Chaput and I. Tanaka, *Phys. Rev. B* **91**,

- 094306 (2015).
- ³¹ A. Togo, F. Oba, and I. Tanaka, Phys. Rev. B **78**, 134106 (2008).
- ³² X. F. Wu, V. Varshney et al., Chem. Phys. Lett. **669**, 233 (2017).
- ³³ R. C. Andrew, R. E. Mapasha, A. M. Ukpong and N. Chetty, Phys. Rev. B **85**, 125428 (2012).
- ³⁴ E. Mariani and F. V. Oppen, Phys. Rev. Lett. **100**, 076801 (2008).
- ³⁵ J. Carrete , W. Li, L. Lindsay, D. A. Broido, L. J. Gallego and N. Mingo, Mater. Res. Lett. **4**, 204 (2016).
- ³⁶ S.I. Tamura, Phys. Rev. B, **27**, 858 (1983).